

Automatic Segmentation of Neonatal Images Using Convex Optimization and Coupled Level Set Method

Li Wang^{1,2}, Feng Shi², John H. Gilmore³, Weili Lin⁴, and Dinggang Shen^{2,*}

¹School of Computer Science & Technology,
Nanjing University of Science and Technology, China

²IDEA Lab, Department of Radiology and BRIC,
University of North Carolina at Chapel Hill, USA

`dgshen@med.unc.edu`

³Department of Psychiatry, University of North Carolina at Chapel Hill, USA

⁴MRI Lab, Department of Radiology and BRIC,
University of North Carolina at Chapel Hill, USA

Abstract. Accurate segmentation of neonatal brain MR images remains challenging mainly due to poor spatial resolution, low tissue contrast, high intensity inhomogeneity. Most existing methods for neonatal brain segmentation are atlas-based and voxel-wise. Although parametric or geometric deformable models have been successfully applied to adult brain segmentation, to the best of our knowledge, they are not explored in neonatal images. In this paper, we propose a novel neonatal image segmentation method, combining local intensity information, atlas spatial prior and cortical thickness constraint, in a level set framework. Besides, we also provide a robust and reliable tissue surfaces initialization for our proposed level set method by using a convex optimization technique. Validation is performed on 10 neonatal brain images with promising results.

1 Introduction

Accurate segmentation of neonatal brain structures from magnetic resonance (MR) images has important implications for normal brain development, as well as for the diagnose and treatment of neurodevelopmental disorders such as prematurity. Manual segmentation of neonatal brain structures is tedious, time consuming, and also lacks of reproducibility. Therefore, it is necessary to use automatic techniques for neonatal brain segmentation. However, despite of the success of segmentation methods developed for adult brain, it still remains challenging to segment neonatal brain images [1,2] due to poor spatial resolution, low contrast, and ambiguous tissue intensity distribution [1,3], as well as the inverted contrast between white matter (WM) and gray matter (GM) [2].

Most existing methods for neonatal brain segmentation are atlas-based and voxel-wise [1,3,4,5,6]. For example, Prastawa *et al.* [1] proposed an atlas-based approach for neonatal brain segmentation. They generated an atlas by averaging three semi-automatic segmented neonatal brain images and adopted the

* Corresponding author.

expectation-maximization (EM) scheme with inhomogeneity correction to achieve tissue classification. Shi *et al.* [3] proposed a framework for performing neonatal brain tissue segmentation by using a subject-specific tissue probabilistic atlas generated from longitudinal data follow-up of the same subject. All the above-mentioned methods for neonatal segmentation, however, are based on voxel-wise segmentation. Geometric information has not been paid much attention in the neonatal brain segmentation. However, geometric information describes the gradient and boundary of tissue structures, constraints the relationship of structural shapes, which is appreciated in tissue segmentation to manage the ambiguous structural distributions, especially in neonatal images.

One of the most effective ways of incorporating geometric information for tissue segmentation is to use active contour/surface models [7]. These models are able to provide smooth and closed contours/surfaces as final segmentation, which is not possible for the voxel-based segmentation methods. In fact, geometrically, the human cerebral cortex is a thin, folded sheet of GM, with a nearly consistent thickness of 1-5 mm for neonatal brains. Therefore, surface-based techniques are considered to be more suitable for neonatal brain segmentation than the voxel-based segmentation methods. To obtain a detailed geometric representation of the cortex, many algorithms have been proposed using explicit or implicit surface representation [8,9,10,11,12]. However, they cannot be directly applied to neonatal brain images.

2 Method

In this paper, we present a novel surface-based method, utilizing local intensity information, atlas spatial prior and cortical thickness constraint, for segmentation of neonatal MR brain images. We adopt the local Gaussian distribution fitting (LGDF) energy [13], which describes local image intensities by Gaussian distributions with different means and variances. The means and variances of local intensities are spatially varying functions, which enable the model to deal with intensity inhomogeneities. A prior knowledge from atlases is then combined with the LGDF energy to regularize the segmentation and further increase its ability of handling inhomogeneities. Based on the fact that the cortex has a nearly constant thickness, a constraint of cortical thickness can provide useful geometric information to guide more accurate segmentation. Accordingly, these three terms are finally incorporated into a coupled surface-based method in such a way that the surfaces are driven by the LGDF and spatial prior, while the distance between the inner and the outer surfaces of cortex remains within a predefined range by the constraint of cortical thickness. The contributions of this paper are three-fold:

- a) We use adaptive mean and variance for the same tissue at different locations of brain, for dealing with the inhomogeneities;
- b) We use atlas prior information to guide the segmentation;
- c) We use coupled surfaces to fit the CSF/GM and GM/WM boundaries with a cortical thickness constraint.

An overview of the proposed framework is shown in Fig. 1. The framework consists of three steps: (1) Preliminary segmentation for CSF, WM and GM, as shown in the right panel of Fig. 1; (2) Partial Volume (PV) removal and correction of the mislabeled CSF from WM, as shown in the bottom panel; and (3) Coupled surface-based segmentation, as shown in the left panel. Steps (1) and (2) form an initialization for the step (3). For better emphasizing our contribution, we will first introduce step (3) in Section 2.1, and then steps (1) and (2) in Sections 2.2 and 2.3, respectively. The following sections describe the method in detail.

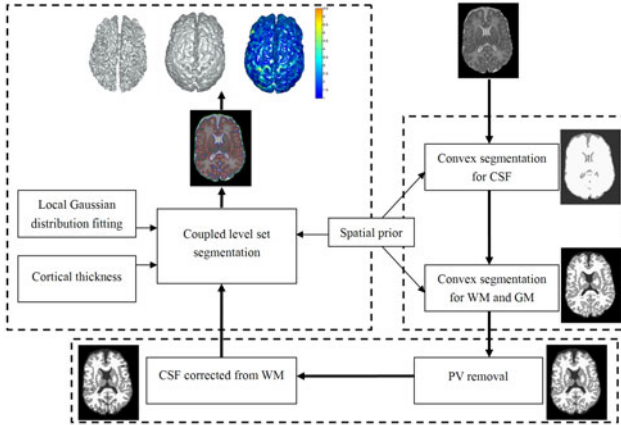


Fig. 1. The proposed framework for neonatal segmentation

2.1 Neonatal segmentation Using Coupled Level Set Method

In this section, we propose an implicit level set method based on local intensity distribution fitting, spatial prior, and cortical thickness constraint for neonatal brain segmentation. Let Ω be the image domain, I be a given image, and $\{\Omega_i\}_{i=1}^N$ be a set of disjoint image regions, such that $\Omega = \cup_{i=1}^N \Omega_i$, $\Omega_i \cap \Omega_j = \emptyset, \forall i \neq j$, where N refers to the number of regions. Based on the work in [13], for each point x in the image domain Ω , the local Gaussian distribution fitting energy is defined as $\mathcal{E}_x^{LGF} = \sum_{i=1}^N \int_{\Omega_i} -\omega_\sigma(x-y) \log p_{i,x}(I(y)) dy$, where $\omega_\sigma(x-y)$ is a Gaussian kernel with a scale parameter σ as proposed in [14,15] and $p_{i,x}(I(y))$ is the probability density, which is defined as $p_{i,x}(I(y)) = 1/(\sqrt{2\pi}\sigma_i(x)) \exp(-(u_i(x) - I(y))^2 / (2\sigma_i(x)^2))$, where $u_i(x)$ and $\sigma_i(x)$ are local intensity means and standard deviations, respectively. It is worth noting that local intensity means $u_i(x)$ and variances $\sigma_i^2(x)$ are the spatially varying functions, which are crucial in handling the inhomogeneity. Due to large overlap in the tissue distribution, it is necessary to use spatial prior for guiding the segmentation. In the following, we propose a new energy function which combines the local Gaussian distribution fitting energy and spatial prior knowledge *prior* _{i} from neonatal brain atlases,

$$\mathcal{E}_x^{L-Prior} = \sum_{i=1}^N \int_{\Omega_i} -\omega_\sigma(x-y) \log(\text{prior}_i(y)p_{i,x}(I(y)))dy \quad (1)$$

The ultimate goal is to minimize $\mathcal{E}_x^{L-Prior}$ for all the center points x in the image domain Ω , which directs us to define an energy function as the following double integral: $\mathcal{E}_x^{L-Prior} = \int \mathcal{E}_x^{L-Prior} dx$. We can use one or multiple level set functions to represent a partition $\{\Omega_i\}_{i=1}^N$. For neonatal segmentation, we use three level set functions ϕ_1 , ϕ_2 and ϕ_3 to represent WM, GM, CSF and background, where the zero level surfaces of ϕ_1 , ϕ_2 and ϕ_3 are interfaces of WM/GM, GM/CSF, and CSF/background, respectively. Let $\Phi = (\phi_1, \phi_2, \phi_3)$. Using Heaviside function H , the energy function based on the LGDF energy and atlas spatial prior can be defined as

$$\mathcal{F} = \int \left(\sum_{i=1}^4 \int -\omega_\sigma(x-y) \log(\text{prior}_i(y)p_{i,x}(I(y))) M_i(\Phi(y)) dy \right) dx + \nu \sum_{i=1}^3 \mathcal{L}(\phi_i) \quad (2)$$

where $\mathcal{L}(\phi_i) = \int |\nabla H(\phi_i(x))| dx$ is the length term to maintain a smooth contour/surface during evolution, and $M_i(\Phi)$ are defined as $M_1 = H(\phi_1)H(\phi_2)H(\phi_3)$, $M_2 = (1-H(\phi_1))H(\phi_2)H(\phi_3)$, $M_3 = (1-H(\phi_2))H(\phi_3)$, and $M_4 = 1-H(\phi_3)$.

Minimization of the energy function \mathcal{F} in Eq. (2) with respect to ϕ_i is achieved by solving the gradient descent flow equations as follows,

$$\begin{aligned} \partial\phi_1/\partial t &= -\delta(\phi_1)H(\phi_2)(e_1-e_2)H(\phi_3) + \nu\delta(\phi_1)K_1 \\ \partial\phi_2/\partial t &= -\delta(\phi_2)(H(\phi_1)(e_1-e_2) + (e_2-e_3))H(\phi_3) + \nu\delta(\phi_2)K_2 \\ \partial\phi_3/\partial t &= -\delta(\phi_3)(H(\phi_2)H(\phi_1)e_1 + H(\phi_2)(1-H(\phi_1))e_2 + (1-H(\phi_2))e_3 - e_4) + \nu\delta(\phi_3)K_3 \end{aligned} \quad (3)$$

where $K_i = \text{div} \left(\frac{\nabla\phi_i}{|\nabla\phi_i|} \right)$ and $e_i(x) = -\log(\text{prior}_i(x)) + \int \omega_\sigma(y-x) [\log(\sigma_i(y)) + \frac{(u_i(y)-I(x))^2}{2\sigma_i(y)^2}] dy$.

As proposed in [9,11], the cortex layer has a nearly consistent thickness which can be used to guide the surface evolutions. To utilize the cortical structural information, we design a coupled surfaces model to constrain the distance of zeros level surfaces of ϕ_1 and ϕ_2 within a reasonable range. Let the allowed distance be $[d, D]$. We adopt the coupling functions $h(\cdot)$ and $c_i(\phi_j)$ in [16,9], where $h(x)$ is a function that $h(x) = 1$ when the distance between the two surfaces is within an acceptable range, otherwise $h(x) = 0$, and $c_i(\phi_j)$ is another coupling function that remains the distance within an acceptable range. Therefore, we write

$$\partial\phi_1/\partial t = h(|\phi_2|) [-\delta(\phi_1)H(\phi_2)(e_1-e_2)H(\phi_3)] + c_1(\phi_2)|\nabla\phi_1| + \nu\delta(\phi_1)K_1 \quad (4)$$

where $h(\cdot)$ and $c_i(\phi_j)$ are defined as

$$h(x) = \begin{cases} 0, & [x \leq d] \cup [x > D]; \\ 1, & [d+f < x < D-f]; \\ 1 - \left(\frac{x-d-f}{f}\right)^2, & [d < x \leq d+f]; \\ 1 - \left(\frac{x-D+f}{f}\right)^2, & [D-f \leq x \leq D]. \end{cases} \quad c_i(\phi_j) = (1-h(|\phi_j|)) \begin{cases} \text{sign}(\phi_j), & |\phi_j| \geq D-f; \\ -\text{sign}(\phi_j), & |\phi_j| \leq d+f. \end{cases}$$

where f is the constant that determines the range of the preferable values for the distance $[d+f, D-f]$ (In all our experiments, we set $f=1$). There are two advantages of this design. First, the image-based force $[-\delta(\phi_1)H(\phi_2)(e_1-e_2)H(\phi_3)]$

guides the surface evolution only when the distance between the two surfaces is within the acceptable range. Second, when the distance is beyond the acceptable range, this force does not affect the evolutions but the second term $c_1(\phi_2)|\nabla\phi_1|$ is activated which will deflate the surface if the distance is below the minimum acceptable value, and inflate the surface if the distance is beyond the maximum acceptable value.

In a similar way, we write a new evolution equation for ϕ_2 ,

$$\partial\phi_2/\partial t=h(|\phi_1|)[- \delta(\phi_2)(H(\phi_1)(e_1-e_2)+(e_2-e_3)H(\phi_3))+c_2(\phi_1)|\nabla\phi_2|+\nu\delta(\phi_2)K_2] \quad (5)$$

With the combination of local Gaussian distribution fitting energy, spatial prior knowledge, and cortical thickness constraint, the proposed method is able to achieve accurate segmentation for neonatal MR images. However, as 3D convolution operations are performed every iteration, the proposed method is computationally expensive. A good initialization for the proposed method is not only necessary to save time but also help avoid being trapped into local minima. In the following section, we will propose a robust initialization method based on convex optimization.

2.2 Preliminary Segmentation for CSF, WM and GM

Due to the fact that CSF has the highest intensity in neonatal T2 brain image, we can first extract CSF from the brain image, and then separate WM from GM. This design is much easier than the extraction of CSF, WM and GM simultaneously as in the conventional methods. To address the issue of inhomogeneity, we adopt a joint segmentation and inhomogeneity estimation scheme. We first logarithmically transform the intensities in order to make the bias b additive. We then use two variables u_1 and u_2 , which take values between 0 and 1, to represent the membership functions of three regions with $M_1 = u_1u_2$, $M_2 = u_1(1-u_2)$, and $M_3 = (1-u_1)$. The intensities of each region are characterized by a global Gaussian distribution with mean and variance as (c_i, σ_i^2) . The atlas spatial prior $prior_i$ is also utilized for segmentation. We then propose the following energy for segmenting the image into the regions of CSF, (WM+GM) and background,

$$E(u_1, u_2, c_i, \sigma_i, b) = - \sum_{i=1}^3 \int \log(prior_i(x)p_i(x))M_i(x)dx + \nu \int |\nabla u_1|dx + \nu \int |\nabla u_2|dx, u_1 \in [0, 1], u_2 \in [0, 1] \quad (6)$$

where $p_i(x) = 1/(\sqrt{2\pi}\sigma_i) \exp(-(\log I(x) - c_i - b)^2/(2\sigma_i^2))$ and the last two terms are the total variation of u_1 and u_2 . By constraining both u_1 and u_2 to be $[0, 1]$, the minimization problem is convex with respect to u_1 and u_2 when (c_i, σ_i, b) are fixed [17,18]. Therefore, we can easily use the Split Bregman method [19] to minimize u_1 and u_2 . The global means c_i and variances σ_i^2 can be easily solved. For fixed $(u_1, u_2, c_i, \sigma_i)$, the bias field b can be determined by $b = \sum_{i=1}^3 ((\log I - c_i)M_i/\sigma_i^2) / \sum_{i=1}^3 (M_i/\sigma_i^2)$. In view of the slowly varying property of the bias field, using the technique in [14], we can derive a smooth bias field in this form, $b = \left((\sum_{i=1}^3 ((\log I - c_i)M_i/\sigma_i^2)) * g \right) / \left((\sum_{i=1}^3 (M_i/\sigma_i^2)) * g \right)$, where

$*$ is the convolution operation, and g is a lowpass filter, such as a mean-filter kernel or Gaussian-filter kernel.

After preliminary segmentation for CSF, we further apply the same scheme to segment the image into WM, GM and background by masking off the CSF. The energy is the same as Eq. (6). With these two convex models, we can achieve a good preliminary segmentation for the neonatal images. For example, Fig. 2(a) shows a slice of neonatal brain. Fig. 2(b) shows the preliminary segmentation result obtained by these convex models.

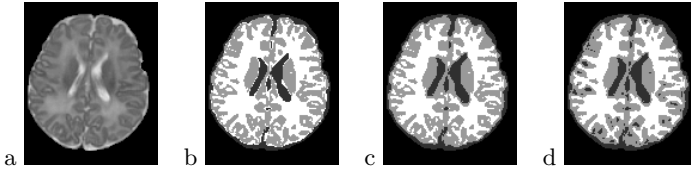


Fig. 2. Demonstration of preliminary tissue segmentation steps. (a) Original slice; (b) Preliminary segmentation; (c) PV removal; (d) Correction of CSF from WM.

2.3 Partial Volume (PV) Removal and CSF Correction from WM

After preliminary segmentation, we find that many voxels between CSF and GM are incorrectly classified as WM due to partial volume effect. In [2], Xue *et al.* proposed a technique based on EM algorithm and Markov random field (MRF) to remove the effect of PV. However, their PV removal strategy is somehow complicated. In this paper, we adopt rather simple but effective scheme to handle PV problem based on the observation that the misclassified WM are commonly surrounded by the CSF and GM. For each segmented WM voxel, in its neighborhood with size of $w \times w \times w$, let the number of WM, GM and CSF/BG be N_{WM} , N_{GM} , and N_{CSF} . If $N_{WM} \leq a$, while $N_{GM} > N_{CSF} \geq b$, then this WM should be set as GM. If $N_{WM} \leq a$, while $N_{CSF} > N_{GM} \geq c$, then this WM should be set as CSF. In this paper, we set $a = 3, b = 3, c = 6, w = 3$ for all experiments. Fig. 2(c) shows the correction result achieved by our PV removal scheme. In our experiment, we also find that there are some CSF voxels in sulci that are incorrectly labeled as WM. In this case, we adopt the scheme proposed in [2], which is based on the observation that these mislabeled CSF are unconnected with true WM volume, to correct these misclassified CSF from WM. Fig. 2(d) shows the correction result for CSF. This preliminary result will be used as a good initialization for the coupled level set method in Section 2.1.

3 Experimental Results

Data were acquired from a 3T Siemens scanner. T2 images of 70 axial slices were obtained with imaging parameters: TR=7380 ms, TE=119 ms, Flip Angle=150, acquisition matrix= 256×128 , and resolution= $1.25 \times 1.25 \times 1.95$ mm³. T2 images

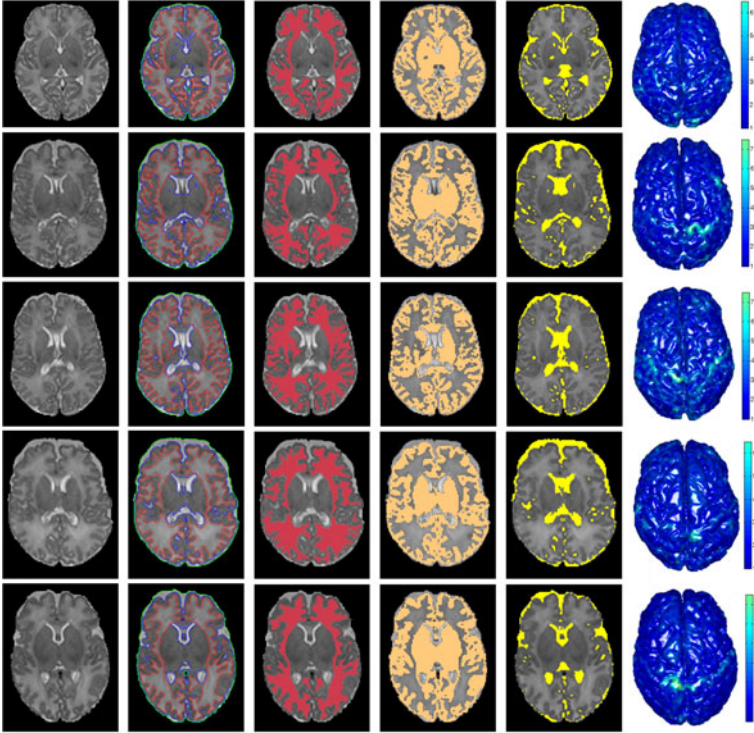
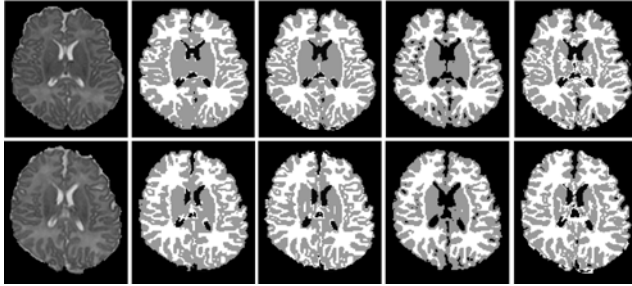


Fig. 3. 3D automatic neonatal brain segmentation results. From left to right: original T2 slices, results by the proposed method, segmented WM, GM, CSF, and thickness between WM/GM and GM/CSF surfaces.

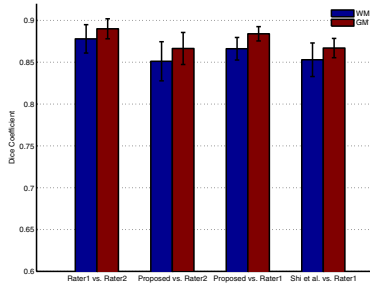
are resampled to $1 \times 1 \times 1 \text{ mm}^3$ before further processing. In our experiments, we set the allowable thickness for cortex as $[1 \ 6.5] \text{ mm}$, $\nu = 0.5$ for Eq. (2), $\nu = 0.25$ for Eq. (6), and $\sigma = 3.0$. The functions δ and H are regularized as in [20]. The level set functions are reinitialized every iteration using fast marching method [21].

Our method has been validated using images obtained from 10 neonates. Due to the page limit, we show only the segmentation results for five subjects in Fig. 3. The first two columns show the original T2 slices and segmentation results of our coupled level set method. To better view the results, we also present the hard segmentations of WM, GM and CSF in columns 3, 4 and 5, respectively. Visual inspection of these results shows that WM, GM and CSF are reasonably well segmented. The last column visualizes the distance (or thickness) between WM/GM surface and GM/CSF surface. It can be seen that most of cortical thickness of these subjects are $[1 \ 5] \text{ mm}$, which is consistent with what we assumed.

Validation of the automatic segmentation results is difficult because ground truth is not available. For comparison, we have to refer to the manual



(a)



(b)

Fig. 4. (a): Segmentation results on two representative subjects. Column 1: original T2 images; columns 2 and 3: manual segmentation results by two experts; column 4: results by our proposed method; Column 5: results by the method of Shi *et al.* (b): Comparison of segmentation accuracy on WM and GM for 10 subjects by different methods.

segmentations by experts as our ground truth. Fig. 4(a) shows the segmentation results of two representative subjects by two expert raters (columns 2 and 3) and by our method (column 4). By visual inspection, our results are comparable with those produced by expert raters. As atlas-based segmentation method is popular for neonatal brain segmentation, we do another comparison with the latest atlas-based segmentation method proposed by Shi *et al.* [3], with their results shown in the last column. To have a fair comparison for GM, we mainly compare the segmentation performance in the cortical regions. We employ Dice Coefficient (DC) [22] to measure the overlapping rate between two segmentations, which is defined as $DC = 2|A \cap B| / (|A| + |B|)$. DC ranges from 0 to 1, corresponding to the worst and the best agreement between labels of two regions. We first compare our results with manual segmentations by two raters. The mean and standard deviation of DC values of the WM and GM segmentations of all 10 subjects are presented in the first three pairs of bars in Fig. 4(b). We can observe that our proposed automatic segmentation method achieves comparable segmentation performance on WM and GM as manual raters. Taking the manual segmentation from rater 1 as ground truth, we then compare with the method of Shi *et al.* [3], and provide the results in the last pair of bars. It can be seen

that our proposed method outperforms the method of Shi *et al.*, by achieving the relatively higher DC values for both WM and GM.

4 Conclusion

We have presented a novel surface-based method for neonatal brain segmentation. Our method effectively utilizes local image information, atlas prior knowledge, and cortical thickness constraint for guiding the segmentation, by integrating them into a coupled level set method. We also provide a robust initialization method using convex optimization for this coupled level set method. Our proposed method has been validated on 10 subjects with promising results. In our future work, we will test our proposed method with more data.

References

1. Prastawa, M., Gilmore, J.H., Lin, W., Gerig, G.: Automatic segmentation of MR images of the developing newborn brain. *Medical Image Analysis* 9(5), 457–466 (2005)
2. Xue, H., et al.: Automatic segmentation and reconstruction of the cortex from neonatal MRI. *NeuroImage* 38(3), 461–477 (2007)
3. Shi, F., et al.: Neonatal brain image segmentation in longitudinal MRI studies. *NeuroImage* 49(1), 391–400 (2010)
4. Warfield, S.K., Kaus, M., Jolesz, F.A., Kikinis, R.: Adaptive, template moderated, spatially varying statistical classification. *Medical Image Analysis* 7(4), 43–55 (2000)
5. Weisenfeld, N.I., Warfield, S.K.: Automatic segmentation of newborn brain MRI. *NeuroImage* 47(2), 564–572 (2009)
6. Cocosco, C.A., Zijdenbos, A.P., Evans, A.C.: A fully automatic and robust brain MRI tissue classification method. *Medical Image Analysis* 7(4), 513–527 (2003)
7. Gooya, A., Liao, H., Matsumiya, K., Masamune, K., Masutani, Y., Dohi, T.: A variational method for geometric regularization of vascular segmentation in medical images. *IEEE Transactions on Image Processing* 17(8), 1295–1312 (2008)
8. Xu, C., et al.: Reconstruction of the human cerebral cortex from magnetic resonance images. *IEEE Trans. Med. Imag.* 18(6), 467–480 (1999)
9. Zeng, X., Staib, L., Schultz, R., Duncan, J.: Segmentation and measurement of the cortex from 3D MR images using coupled surfaces propagation. *IEEE Trans. Med. Imag.* 18(10), 100–111 (1999)
10. MacDonald, D., Kabani, N., Avis, D., Evans, A.C.: Automated 3-d extraction of inner and outer surfaces of cerebral cortex from MRI. *NeuroImage* 12(3), 340–356 (2000)
11. Goldenberg, R., Kimmel, R., Rivlin, E., Rudzsky, M.: Cortex segmentation: a fast variational geometric approach. *IEEE Trans. Med. Imag.* 21(2), 1544–1551 (2002)
12. Han, X., et al.: Cruise: Cortical reconstruction using implicit surface evolution. *NeuroImage* 23(3), 997–1012 (2004)
13. Wang, L., He, L., Mishra, A., Li, C.: Active contours driven by local gaussian distribution fitting energy. *Signal Processing* 89(12), 2435–2447 (2009)

14. Li, C., et al.: A variational level set approach to segmentation and bias correction of medical images with intensity inhomogeneity. In: Metaxas, D., Axel, L., Fichtinger, G., Székely, G. (eds.) MICCAI 2008, Part II. LNCS, vol. 5242, pp. 1083–1091. Springer, Heidelberg (2008)
15. Li, C., Kao, C., Gore, J., Ding, Z.: Implicit active contours driven by local binary fitting energy. In: CVPR, pp. 1–7 (2007)
16. Paragios, N.: A variational approach for the segmentation of the left ventricle in mr cardiac images. In: VLSM 2001 (2001)
17. Bresson, X., et al.: Fast global minimization of the active contour/snake model. *J. Math. Imaging Vis.* 28(2), 151–167 (2007)
18. Chan, T.F., Esedoglu, S., Nikolov, M.: Algorithms for finding global minimizers of image segmentation and denoising models. *SIAM J. Appl. Math.* 66(5), 1632–1648 (2006)
19. Goldstein, T., Bresson, X., Osher, S.: Geometric applications of the split bregman method: Segmentation and surface reconstruction. CAM Report 09-06, UCLA (2009)
20. Chan, T., Vese, L.: Active contours without edges. *IEEE Trans. Imag. Proc.* 10(2), 266–277 (2001)
21. Sethian, J.: *Level Set Methods and Fast Marching Methods*. Cambridge University Press, Cambridge (1999)
22. Dice, L.: Measures of the amount of ecologic association between species. *Ecology* 26, 297–302 (1945)